Photoluminescence in ZrO_2 doped with Y and La

(Fotoluminescência em ZrO_2 dopado com Y e La)

W. S. C. de Sousa[1], D. M. A. Melo[2], J. E. C. da Silva[3], R. S. Nasar[1], M. C. Nasar[1], J. A. Varela[3]
[1]Departamento de Química, UFRN, Natal, RN 59072-970
[2]Universidade Federal do Tocantins, Araguaína, TO 77807-060
[3]Universidade Estadual Paulista - UNESP, Araraquara, SP 14800-900
nasar@terra.com.br

Abstract

This study aims to describe the synthesis and optical characterization of a nanometric zirconium oxide solid solution containing yttrium and lanthanum. Zirconium citrate, yttrium nitrate and lanthanum nitrate were mixed in the ratios: 94 mol% of ZrO_2 - 6 mol% of Y_2O_3 and 92 mol% of ZrO_2 - 6 mol % of Y_2O_3 - 2 mol % of La_2O_3. FTIR analysis shows organic material in decomposition and thermal analysis shows the transformation from the tetragonal to the monoclinic phase of zirconia, the loss of water molecule and zirconium dehydroxylation. The X-ray diffraction analysis shows a homogeneous phase formation of ZrO_2-Y_2O_3-La_2O_3 demonstrating that lanthanum addition does not cause phase formation, promoting a solid solution based on zirconia with cubic structure. The photoluminescence spectra show absorption bands at 562 nm and 572 nm (350 °C) and specific absorption bands at 543 nm, 561 nm, 614 nm and 641 nm (900 °C). The photoluminescence effect at low temperature is caused by defects such as $(Y_{Zr},Y_O)'$, $(2Y_{Zr},V_O)''$ and V_O. Emissions at 614 nm and 641 nm are caused by O-2p → Zr-4d transition. An emission at 543 nm can be attributed to LaO_8 centers with O-2p → La-5d transition.
Keywords: photoluminescence, yttria-stabilized zirconia, Pechini method.

Resumo

O objetivo deste trabalho é descrever a síntese e a caracterização óptica de uma solução sólida de óxido de zircônio contendo ítrio e lantânio. Foram misturados citrato de zircônio, nitrato de ítrio e nitrato de lantânio nas proporções 94 mol% ZrO_2-6 mol% Y_2O_3 e 92 mol% ZrO_2-6 mol % Y_2O_3-2 mol % La_2O_3. A análise de espectroscopia de absorção no infravermelho com tranformada de Fourier mostra material orgânico em decomposição e a análise térmica mostra a transformação de fases da zircônia tetragonal para monoclínica, a perda de água e a desidroxilação do zircônio. A análise por difração de raios X mostra formação de fases homogênea de ZrO_2-Y_2O_3-La_2O_3 demonstrando que a adição de lantânio não provoca formação de fases, promovendo uma solução sólida baseada em zircônia cúbica. Os espectros de fotoluminescência mostram bandas de absorção em 562 nm e 572 nm (350 ºC) e bandas de absorção específicas em 543 nm, 561 nm, 614 nm e 641 nm (900 ºC). O efeito fotoluminescente a baixas temperaturas é causado por defeitos como $(Y_{Zr},Y_O)'$, $(2Y_{Zr},V_O)''$ e V_O. As emissões em 614 nm e 641 nm são causadas pela transição O-2p → Zr-4d. Uma emissão em 543 nm pode ser atribuída a centros LaO_8 com transição O-2p → La-5d.
Keywords*: fotoluminescência, zircônia estabilizada com ítria, método Pechini.*

INTRODUCTION

The preparation of stabilized zirconia by chemical methods has attracted a great deal of interest. Several preparation techniques based on solution chemistry methods, such as coprecipitation [1], sol-gel [2], self-combustion [3], colloidal chemistry [4] and polymeric precursors [5] have been attempted for the preparation of highly homogeneous and fine powder of stabilized zirconia. Various works have been done on zirconia stabilization with Ca, Mg, Ce, Y and other additions [6-8] into the zirconia structure. Substitutions of zirconium by yttrium caused solid solution formation with vacancies creation and stabilized the tetragonal and cubic forms depending on yttrium concentration. Additions of 8 mol % Y_2O_3 or 12 mol % MgO and CaO in zirconia [9] stabilized the cubic structure with a homogeneous phase. YSZ Crystals (yttrium-stabilized zirconia) show a tetragonal structure that varies from 200 °C to 1200 °C. Ternary systems, such as ZrO_2-Y_2O_3 with additions of TiO_2 [10], CeO_2 [11], Ta_2O_5 [12], Nb_2O_5 [12], HfO_2 [12] and Sc_2O_3 [13] stabilized the tetragonal form of the zirconia structure.

Recent studies about zirconate phases show that zirconium is optically active [14]. However, systems with yttrium addition do not show optical characteristics.

The lanthanides series (Ln) are elements characterized by gradual occupation of 4f orbital. The electronic configuration

of these elements are [Xe] $4f^n$ with n=0 (lanthanum) and n=14 (lutecium). Both elements do not present positions of optically active lattice.

It was observed that the addition of lanthanum does not stabilize zirconia [9]. According to Zeng et al. [15], the addition of lanthanum and niobium in zirconia caused a formation of phases such as $La_2Zr_2O_7$, La_3NbO_7 and $LaNb_3O_9$. A model proposed by researchers from the National Bureau of Standards (NBS) considers that additions of lanthanum in zirconia caused a pyrochlore phase formation, $A_2B_2O_7$ type, and solid solution [16]. Dietzel and Tober [17] developed a model considering field strength of compounds. According to the model, the lanthanum addition in zirconia caused phase formation.

In this study, a small concentration of yttrium and lanthanum is added to the zirconia phase by a polymeric precursor method proposed by Pechini [18]. The stability of the formed phases is systematically observed and the photoluminescence characteristics of the phase analyzed.

EXPERIMENTAL PROCEDURE

Synthesis

Citric acid and zirconium propoxide, (Table I), were mixed under stirring at 90 °C/8 h for zirconium citrate formation. Pure ethylene glycol was added to the solution and homogenized at 90 °C for 2 h. The resin of zirconium and yttrium nitrate were mixed in two ratios under magnetic agitation at 85 ºC for 2 h, one of the mixes had 94 mol% of ZrO_2 and 6 mol% of Y_2O_3, ZY, and the other one 92 mol% of ZrO_2 and 6 mol% of Y_2O_3, ZYL. To the second mixture 2 mol% of La_2O_3 was added by agitation in the lanthanum nitrate form. The polymeric resin was calcined at different temperatures and times.

Table I - Origin and purity of reagents.
[Tabela I - Origem e pureza dos elementos.]

Reagent	Origin	Purity (%)
Zirconium propoxide	NOAH	99.9
Citric acid	REAGEN	99.5
Etyleneglycol	REAGEN	99.5
Lanthanum nitrate	VETEC	99.9
Yttrium nitrate	ALDRICH	99.9

Characterization

The resin was decomposed at 130 °C, 250 °C and 350 °C/3.5 h and the resultant powder was ground in an agate mortar. The powder was calcined between 400 °C and 900 °C for 1, 2 and 4 h.

The polymer vibration bands decomposed at 350 °C/3.5 h were analyzed with a Perkin Elmer FTIR model 16 PC with a spectral range from 4000 cm^{-1} to 400 cm^{-1}. The polymer decomposition and crystallization were analyzed with a DTA/TGA Perkin Elmer model DTA-7 with a 5 °C/min rate.

The powder was analyzed by X-ray diffraction, Siemens D5000, with CuKα radiation of 1.5418 Å. The surface area (SA) and the average crystal size (ACS) were determined by a BET Quantachrome NOVA 2000 and a Cilas - 1064, respectively.

Luminescence effect

Photoluminescence spectra were taken with a U1000 Jobin-Yvon double monochromator coupled to a cooled GaAs photomultiplier and a conventional photon counting system. The 488 nm exciting wavelength of an argon ion laser was used. The maximum output of the laser was 500 mW and a cylindrical lens was provided to prevent the sample from overheating. The slit used was 250 μm and all measurements were taken at room temperature.

RESULTS AND DISCUSSION

The infrared analysis, Fig. 1, of the ZYL polymeric resin shows two absorption bands that vary from 3423 cm^{-1} to 3410 cm^{-1} and 3223 cm^{-1} to 3178 cm^{-1} related to the stretching of OH^- groups of citrates and water molecules co-coordinated metals. Weak bands varying from 2970 cm^{-1} to 2968 cm^{-1} were attributed to OH^- that was linked to carboxylic acid. The band from 2379 cm^{-1} to 2377 cm^{-1} is related to atmospheric CO_2 adsorbed in metallic cations. The bands in the regions from 1607 cm^{-1} to 1575 cm^{-1} and 1404 cm^{-1} to 1398 cm^{-1} correspond to symmetric and asymmetric stretching of COO^- groups. Stretching vibration of ZrO-C is

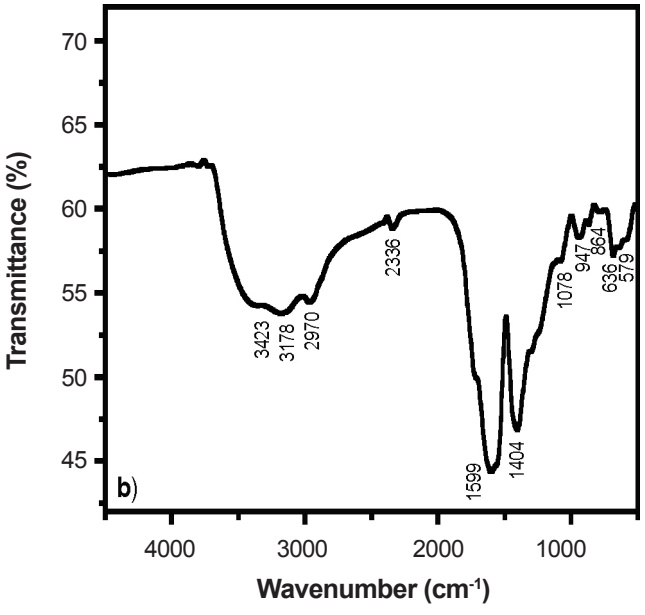

Figure 1: Infrared analysis of the polymeric resin calcined at 250 °C/2 h.
[Figura 1: Análise por infravermelho da resina polimérica calcinada a 250 °C/2 h.]

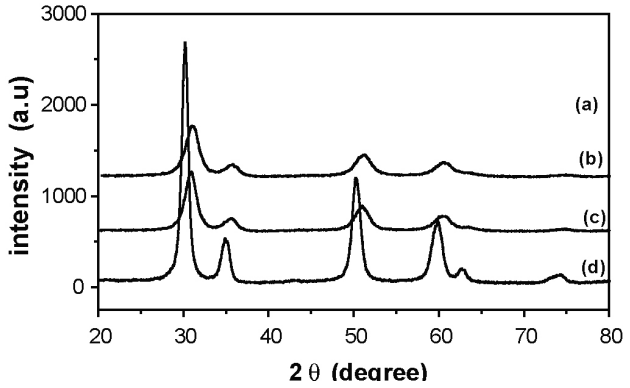

Figure 2: TGA-DTG analysis of powder calcined at 200 °C/2 h.
[Figura 2: Análises termogravimétrica e térmica diferencial do pó calcinado a 200 °C/2 h.]

observed from 1097 cm^{-1} to 1076 cm^{-1}. Bands in 952 cm^{-1} to 945 cm^{-1} regions are due to C-C stretching vibration from 864 cm^{-1} to 856 cm^{-1} and 648 cm^{-1} to 568 cm^{-1}. Bands of ionic CO_3^{2-} (oxycarbonates) and stretching of Zr-O are observed.

Fig. 2 shows TG-DTG analysis of ZYL polymeric resin calcined at 200 °C/2 h with different stages of mass loss initiating the decomposition at 35°C and ending at 728 °C with 73.9% of total mass loss.

Differential thermal analysis of ZYL, Fig. 3, shows the same transformations observed in TG-DTG with an endothermic peak from 35 °C to 148 °C related to loss of water. The polymer decomposition occurred with an endothermic peak between 168 °C and 262 °C, and a carbonaceous phase decomposition is observed from 319 °C to 410 °C with an exothermic peak. The dehydroxylation of the zirconium due to the carboxylic acid is observed by an exothermic peak of 420 °C up to 510 ºC. A decrease of the DTA curve between 580 °C and 630 °C is due to the crystallization of the zirconia phase. It is not clear the transformation from monoclinic to tetragonal phase near 1200 °C.

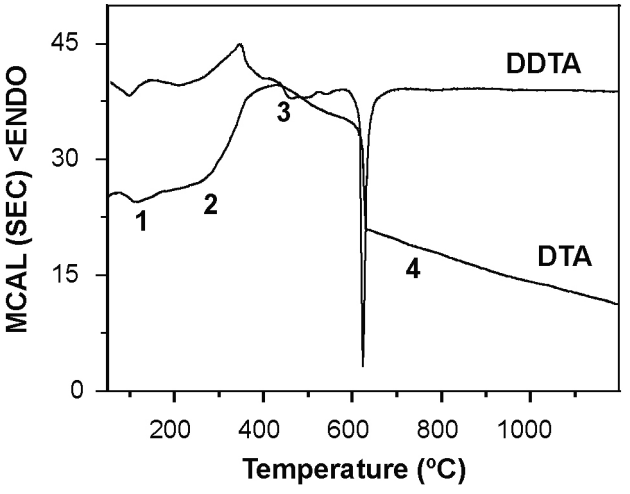

Figure 3: DTA analysis of powder calcined at 200 °C/2 h.
[Figura 3: Análise térmica diferencial do pó calcinado a 200 °C/2 h.]

Phase formation

Fig. 4 shows the X-ray diffraction pattern of ZrO_2-Y_2O_3 solid solution powder calcined at 400 °C/7 h (Fig. 4a) and calcined at 700 °C/7 h (Fig. 4b) with formation of cubic zirconia. Residues of monoclinic and tetragonal structure were not formed. Additions of yttrium into the zirconia structure caused vacancy formation according to the reaction:

$$Y_2O_3 \xrightarrow{ZrO_2} 2Y_{Zr}^{i} + V_o^{\cdot\cdot}\frac{3}{2}O_2 \qquad (A)$$

Some authors consider the solid solution formation and vacancy creation as the cause of zirconia stabilization.

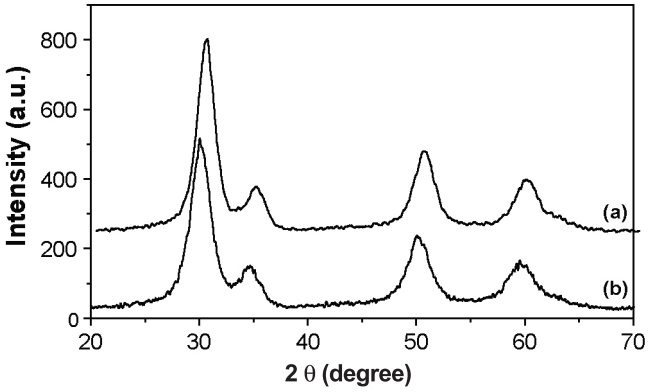

Figure 4: X- ray diffraction patterns of ZrO_2-Y_2O_3-La_2O_3 calcined powder; a) 400 °C/7 h, b) 700 °C/7 h.
[Figura 4: Difratogramas de raios X de pós calcinados de ZrO_2-Y_2O_3-La_2O_3; a) 400 °C/7 h, b) 700 °C/7 h.]

Analysis by XRD, Fig. 5, of ZrO_2-Y_2O_3-La_2O_3 (ZYL) calcined at 400 °C/ 7 h (Fig. 5a) and calcined at 700 °C/7 h (Fig. 5b) shows the same phases observed in the ZY solid solution. Fig. 6 shows the XRD of ZYL solid solution calcined at 900 °C/6 h (Fig. 6d), 700 °C/6 h (Fig. 6c), 600 °C/6 h (Fig. 6b) and 500 °C/6 h (Fig. 6a) demonstrating a high crystallinity with formation of tetragonal and cubic zirconia at 500 °C, 600 °C and 700 °C, and monophase cubic zirconia at 900 °C.

Phases related to lanthanum additions, showing zirconium substitutions by lanthanum that probably occurred into the lattice, were not observed. The addition of lanthanum and yttrium caused a competition during Zr substitutions into the lattice. The yttrium with ionic radius 0.88 Å replaced zirconium preferentially and the lanthanum with ionic radius 1.061Å replaced zirconium more slowly causing segregation. Lanthanum addition forms a solid solution according to the reaction below:

$$La_2O_3 \xrightarrow{ZrO_2} 2La_{Zr}^{i} + V_o^{\cdot\cdot}\frac{3}{2}O_2 \qquad (B)$$

The vacancy brings local tensions of the lattice into

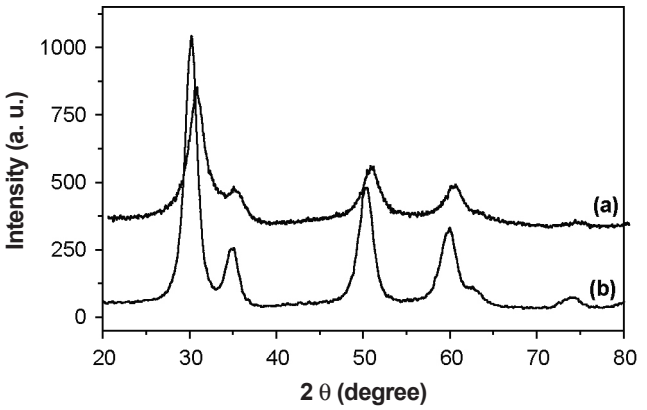

Figure 5: X- ray diffraction of ZrO_2-Y_2O_3-La_2O_3 powder calcined at a) 400 °C/7 h and b) 700 °C/7 h.
[Figura 5: Difratogramas de raios X de pós de ZrO_2-Y_2O_3-La_2O_3 calcinado a 400 °C/7 h (a) e 700 °C/7 h (b).]

relief and increases the phase stability. Models of zirconia stabilization proposed by the NBS researchers [16] and Dietzel and Tober [17] consider the lanthanum addition as a phase former.

Photoluminescence effect

Analyses of ZYL powder calcined at 350 º/7 h, Fig. 7, show high photoluminescence (PL) intensity with a broad band at 562 nm (350 ºC/3.5 h) and 572 nm (350 ºC/7 h), respectively. A small peak of crystallinity is observed by XRD at 350 °C and bands of organic material were observed by FTIR and DTA-TGA (decomposition). The total luminescent effect is due to the state of powder with a non-defined structure and high defect concentration that caused emissions. Kunz et al. [19] proposed that emissions occur in small length waves attributed to powder surface defects and oxygen vacancies. Liang et al. [20] proposed that the defects concentration depends on the method of preparation and the type of excitation of the sample.

The surface area and the average crystal size of calcined powder of the LZT phase, (Table II) show small particles (4.0 nm) with a high surface area at 350 ºC/7 h (78.5 m^2/g). The small size of particle has high defects concentration, such as $(Y_{Zr},V_O)'$, $(2Y_{Zr},V_O)''$ and V_O that in accordance with some authors cause optical properties in YSZ [21-23].

The PL intensity of the powder calcined at 900 ºC/6 h, Fig. 8, shows a narrow specific absorption at 543 nm, 561 nm, 614 nm and 641 nm, respectively. The appearance of bands at 614 nm and 641 nm are related to oxygen positions' perturbation into the structure. An imperfect system caused transitions of O-2p → Zr-4d type. Such behavior was observed by Camagni et al. [24] for yttrium-stabilized zirconia. Other selective emissions and absorption of specific frequencies such as absorption band at 561 nm can be connected with the presence of impurities and imperfections, which provide localized energy levels in the forbidden energy gap. Such impurities called activators contribute to energy levels that are responsible for the emission of visible light.

Lanthanum does not exhibit luminescence effect due to non-existence of f-f transitions. However, a broad peak is observed at 543 nm not occurring in ZrO_2-Y_2O_3. Emissions of La in the zirconia structure can be attributed to LaO_8

Table II - Surface area (sa-m^2/g) and averange crystal size (ACS-nm)
[Tabela II -

Temperatura	SA (m^2/g)	ACS (nm)
350 ºC / 6 h	78,5	4.0
500 ºC / 6 h	67.9	4.2
600 ºC / 6 h	39.0	4.6
700 ºC / 6 h	34.9	5.0
900 ºC / 6 h	10.7	9.0

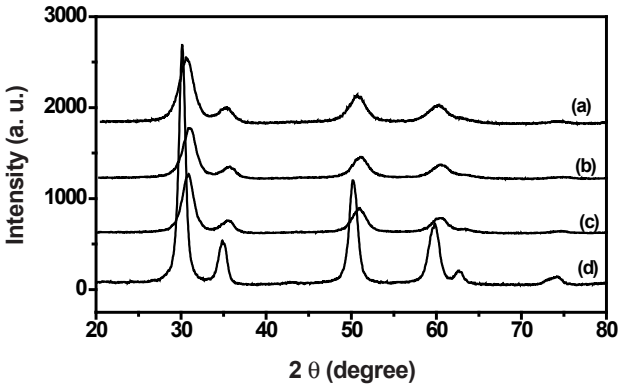

Figure 6: X-ray diffraction patterns of $ZrO_2.Y_2O_3.La_2O_3$ calcined powder. a) 500 °C/6 h; b) 600 °C/6 h; c) 700 °C/6 h; d) 900 °C/6 h.
[Figura 6: Difratogramas de raios X de pós calcinados de $ZrO_2.Y_2O_3.La_2O_3$. a) 500 °C/6 h; b) 600 °C/6 h; c) 700 °C/6 h; d) 900 °C/6 h.]

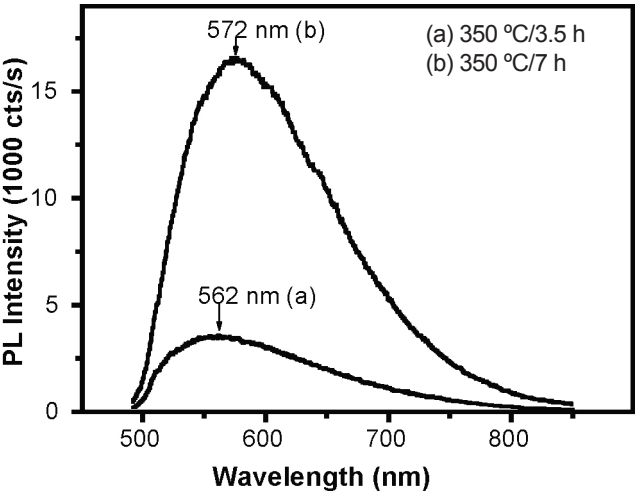

Figure 7: Photoluminescence of calcined powder: a) 350 °C/3.5 h; b) 350 °C/7 h.
[Figura 7: Fotoluminescência do pó calcinado: a) 350 °C/3,5 h; b) 350 °C/7 h.]

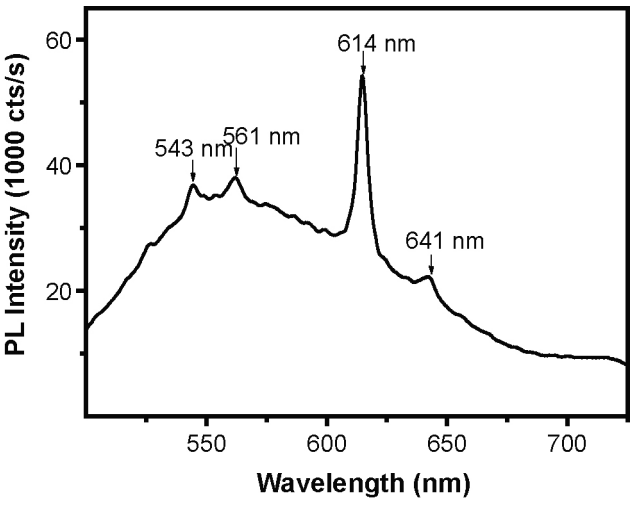

Figure 8: Photoluminescence of powder calcined at 900 °C/6 h.
[Figura 8: Fotoluminescência do pó calcinado a 900 °C/6 h.]

centers. Transitions of the type O-2p → La-5d caused emissions into the structure. Campet et al. [25] studied the photoluminescence of $La_2Ti_2O_7$ observing the same phenomenon.

CONCLUSIONS

A solid solution of ZrO_2-Y_2O_3-La_2O_3 was synthesized with the Pechini method from the polymer decomposition. Non-typical phases based on zirconium, yttrium and lanthanum were observed due to the addition of lanthanum into the ZrO_2-Y_2O_3 system. The analysis of the particle size showed a nanometric particle formation (78 m^2/g and 4 nm) that caused an increase of defect concentrations, such as $(Y_{Zr}, V_O)^{\cdot}$, $(2Y_{Zr}, Vo)^{\cdot\cdot}$ and V_O that contributed to the ZrO_2-Y_2O_3.La_2O_3 optical properties.

PL analyses of powder calcined at 900 °C show emissions at 614 nm and 641 nm attributed to oxygen positions' perturbation causing transition of the O-2p → Zr-4d type. An absorption band at 561 nm is attributed to impurities and imperfections and a broad peak observed at 543 nm is due to LaO_8 centers formation with emissions of O-2p → La-5d type.

REFERENCES

[1] Y. Gu, G. Li, G. Meng, D. Peng, Mater. Res. Bull. **35** (2000) 297.
[2] T. Okubo, H. Nakamoto, J. Mater. Sci. **30** (1995) 749.
[3] S. Roy, W. Sigmund, F. Aldinger, J. Mater. Res. **14**, 4 (1999) 1524.
[4] A. Celikkaya, M. Akine, J. Colloid Interface Sci. **122** (1988) 110.
[5] M. Cerqueira, R. S. Nasar, E. R. Leite, E. Longo, J. A. Varela, Ceram. Int. **26** (2000) 231.
[6] W. T. Smoot, J. R. Ryan, J. Am. Ceram. Soc. **46**, 12 (1963) 597.
[7] E. K. Koehler, Ceram. Int. **10**, 2 (1984) 66.
[8] Y. Ikuma, Y. Tsubaki, T. Masaki, J. Am. Ceram. Soc. **99**, 1 (1992) 99.
[9] I. Abrahan, G. Gritzner, J. Mater. Sci. Lett. **12** (1995) 53.
[10] G. Bayer, J. Am. Ceram. Soc. **53**, 5 (1970) 294.
[11] A. E. Mehale, R. S. Roth, J. Am. Ceram. Soc. **69**, 11 (1986) 827.
[12] D-J Kim, J. Am. Ceram. Soc. **73**, 1 (1990) 115.
[13] F. T. Ciacchi, S. P. S. Badwal, J. Drenan, J. Eur. Ceram. Soc. **7** (1991) 185.
[14] G. F. G. Freitas, R. S. Nasar, M. Cerqueira, D. M. A. Melo, E. Longo, P. S. Pizani, J. A. Varela, Ceram. Int. **29** (2003) 793.
[15] C. Zheng, A. R. West, Br. Ceram. Trans. J. **89** (1990) 138.
[16] R. S. Roth, J. Research Natl. Bur. Standards **56**, 1 (1956) 17; RP 2643.
[17] A. Dietzel, H. Tober, Ceram. Abstr. (Jan. 1954) p. 23a.
[18] M. P. Pechini, U. S. Patent 3,330,000 (1967).
[19] M. Kunz, H. Kretschmann, W. Assmus, C. Klingshirn, J. Lumin. **37** (1987) 123.
[20] J. Liang, J. Mater. Res. Bull. **38** (2003) 161.
[21] J. Liang, Z. Deng, X. Jiang, F. Li, Y. Li, Inorg. Chem. Commun. **41** (2002) 3302.
[22] R. E. W. Casselton, Phys. Status Solidi **2** (1970) 571.
[23] Z. Wang, Z. Q. Chen, J. Zhu, S. J. Wang, X. Guo, Rad. Phys. Chem. **58** (2000) 697.
[24] P. Camagni, P. Galinetto, G. Samoggia, Solid State Commun. **83**, 11 (1992) 943.
[25] G. Campet, J. Claverie, P. Salvador, J. Phys. Chem. Solids **44** (1983) 925.
(Rec. 14/08/2006, Ac. 02/01/2007)